KSCE Journal of Civil Engineering (2020) 24(4):1255-1267
DOI 10.1007/s12205-020-0923-3

pISSN 1226-7988, eISSN 1976-3808
www.springer.com/12205

Structural Engineering

Mechanical Behavior in Perfobond Rib Shear Connector with UHPC-Steel Composite Structure with Coarse Aggregate

Maojun Duan[a], **Shiyu Zhang**[a], **Xu Wang**[b], **Fenghui Dong**[a]

[a]*College of Civil Engineering, Nanjing Forestry University, Nanjing 210037, China*
[b]*College of Civil Engineering, Southeast University, Nanjing 211189, China*

ARTICLE HISTORY

Received 23 May 2019
Revised 8 December 2019
Accepted 6 February 2020
Published Online 11 March 2020

KEYWORDS

Shear capacity
Perfobond rib shear connector
Ultra high performance concrete
Timoshenko beam
Finite-element analysis

ABSTRACT

Using experimental and numerical analysis, this paper aims at investigating the mechanical behavior in Perfobond rib (PBL) shear connectors with ultrahigh-performance concrete (UHPC)-steel composite structures. Twelve push-out specimens fabricated according to the design used for the connectors in the UHPC-steel composite structures in bridges have been investigated. The main objective of this paper was to discuss the mechanism of failure and the influence of different parameters on PBL shear connectors mechanical properties, including the diameter of transverse rebar, hole spacing and number of holes. The results showed that the failure mode of this type is different from that of conventional concrete specimens. During the failure of specimens, there are few cracks and the overall stiffness still maintain a high level, and reveal that a balance between the size of transverse rebar and the diameter of the hole. In addition, the basic form of the ultimate bearing capacity of existing PBL shearing bonds is summarized, and a new concept of steel fiber shearing in UHPC is proposed. Finally, based on the elastic foundation beam model, the full curve calculation formula of UHPC single-hole PBL shear bond is derived by using Timoshenko beam element. The formula calculation results are in good agreement with the experimental values.

1. Introduction

With the development of industrial technology, new civil engineering structures are emerging (Wei et al., 2019; Xu et al., 2019). As a new way of structural composition, composite structure is becoming more and more popular (Zeng et al., 2020). Steel-concrete composite bridge is a new type of bridge structure that maximizes the material advantages of steel and concrete through reasonable mechanical distribution principle (Chen et al., 2013). Compared with steel bridges, the height and the deflection of steel-concrete composite bridge are also reduced. At the same time, the advantages of cost, large span and fast construction make steel-concrete composite bridges world used widely (Nie et al., 2012). In order to maximize the performance of the two materials, it is critical to ensure a reliable connection between the steel and concrete interface (Tian et al., 2019). As one of the effective and convenient construction methods, the stud connector has received a lot of researches and applications at this stage. However, the stud connectors have lower bearing capacity and poor fatigue performance, and the anchoring ability is insufficient for areas with large stress amplitudes (Shariati, 2012).

In the 1980s, Prof. Leonhardt of the University of Stuttgart, Germany, first proposed the concept of Perfobond strip (PBL) connector by welding open-hole steel plates on steel flanges and using concrete dowel to resist shear flow (Leonhardt et al., 1987). Due to its excellent bearing capacity and fatigue performance, PBL shear connectors have low requirements for installation equipment, and soon replaced the stud connectors as the main conveyor for the steel-concrete bridge connection section and anchorage zone. For example, the PBL shear connectors were used in the Nanjing third Yangtze river bridge, Nanjing fourth Yangtze river bridge, and Nujiang bridge.

In order to study the mechanical behavior of PBL shear connector, many scholars have conducted experimental research and numerical simulation analysis. Oguejiofor and Hosain (1997) firstly studied the factors affecting the bearing capacity through 61 test specimens. The conclusion that the optimal

CORRESPONDENCE Fenghui Dong tongjidfh@163.com College of Civil Engineering, Nanjing Forestry University, Nanjing 210037, China

spacing between the holes is 2.25 times the diameter of the holes was given. Nishiumi et al. (1999) defined the effect of the transverse rebar as a lateral constraint, and the yielding of the steel bar was effective when the lateral restraint force is maximum. Medberry and Shahrooz (2002) took into account the influence of the thickness of the perforated steel plate, the width of the flange plate and the length of the steel concrete connection segment on the bearing capacity of the PBL specimens. Existing studies have shown that the PBL shear connector and the stud connector work the same way. The external load is converted into shear deformation of the shear bond to achieve the purpose of transferring load (Zhang et al., 2017b). The biggest difference between them is the difference in the force transmission mechanism. Except for the effect of the transverse reinforcing bar, the concrete dowel also plays a big role in the shear resistance of the PBL shear connector (Di et al., 2018). In recent years, the PBL shear connector are investigated by different researchers. Wang et al. (2017) designed 33 push-out specimens, and the test results showed that the shear capacity of these connectors increased with an increase in the diameter of the transverse reinforcing bar, an increase in the size of the rib holes, and an increase in thickness of the perforated rib plate. Di et al. (2018) indicated that, under a high level of confinement of a concrete dowel, increasing the geometrical size of the hole can improve its bearing capacity significantly without weakening its ductility. Al-Shuwaili (2018) studied the effect of size effect on the static performance of PBL shear bond. The results show that the overall size of the test piece has little effect on the ultimate bearing capacity of PBL shear bond, and the open hole has the highest influence on shear capacity. Zhang et al. (2017a; 2018) have done some researches on PBL shear connector group and fatigue performance. This provided an efficient way for analyzing and designing a PBL shear connector group. Li et al. (2018) proposed an analytical model based on the physical tests to describe the mechanical behavior of multi-hole PBL shear connectors with the assumption of a Lorentzian distributed strain on the perforated steel plate and surrounding concrete. Zhao et al. (2018) concluded that the bearing capacity of the PBL shear bond is mainly derived from the adhesion force, the interface friction force, the dowel effect and the end support force.

In order to further improve the mechanical properties of PBL shear connector, some researchers tried to improve performance from the perspective of structure. Su et al. (2014) investigated the influence of hole diameter by 7 groups of 21 new structured PBL shear connectors, and analyzed the mechanism of shear failure. In summary, for such shaped PBL shear connectors, the main features can be understood as the spatial change of the shape of the perforated steel plate, thereby increasing the mechanical occlusal area of the perforated steel plate and concrete, and improving the shear capacity. However, this type of structure is cumbersome to construct compared to the traditional PBL shear connector, the bearing capacity is not improved significantly, and the economy is insufficient. Chung et al. (2016) studied the failure mode of T-shaped PBL shear bond and gave the calculation formula of shear capacity. Kim et al. (2018) conducted a large number of static tests and hysteresis test analysis on Y-shaped PBL shear bonds, and established a new structure of shear connector system.

With the breakthrough of new cement-based materials and the improvement of manufacturing process, Ultra High Performance Concrete (UHPC) has gradually been applied to the construction of bridge engineering. Compared with the mechanical properties of the PBL shear connector from the structural point of view, the use of UHPC as a casting material can significantly improve its bearing capacity and durability, and has little effect on the constructability. Currently, Sakata-Mirai Footbridge in Japan (Tanaka et al., 2010), Sun-Yu Pedestrian Arch Bridge in Korea (Huh and Byun, 2014) all use the UHPC as construction material. FHWA has conducted extensive research on UHPC bridges since 2001, optimized the development of UHPC “waffle” bridge decks, and published the design guide for UHPC bridge decks in 2013 (Aaleti et al., 2013). Li et al. (2015) and Shao et al. (2018) studied steel-UHPC composite beams, in which the shearing connectors were in the form of studs and steel meshes. Studies have shown that the composite cracking stress of composite beams using UHPC is significantly improved, and their ultimate bearing capacity and fatigue performance are both improved. He et al. (2017; 2018) used UHPC as the PBL shear connector’s grouting slurry. The test results show that the bond strength of the specimen and the concrete “dowel effect” are significantly improved.

The bridges currently used by UHPC are usually small-span bridges, and the incorporation of coarse aggregates is avoided. But with the development of the economy and the improvement of social needs, there will be more and more large bridges. For the anchorage zone or the joint section of a large bridge, the coarse aggregate has an advantage for improving the local mechanical properties. At the same time, there is a large shear force in these regions, making the PBL shear connector more suitable for the system, thereby also causing the complex stress distribution.

This paper intends to study the shear mechanism of PBL shear bond in the steel-UHPC composite structure using coarse aggregate from the perspective of multi-factors. The study will be conducted in the following order:

1. The material test analysis of UHPC formation and force mechanism could give the foundation of superiority and members of UHPC.
2. Through the experimental study, the failure mode, load-slip curve characteristics and bearing capacity of PBL shear connector in steel-UHPC components will be studied.
3. The finite element method is used to verify the optimal hole distance between the PBL shear connectors to make up for the lack of experiments, and to provide ideas for the calculation formula of bearing capacity.
4. From the mechanism point of view, the calculation formula of shear stiffness of PBL shear connector considering shear deformation will be derived, and the theory of calculation formula of existing bearing capacity is improved.

2. Test Overview

2.1 Specimen Size

According to EUROCODE 4 (2014), 4 sets of 12 PBL shear connector specimens were designed and manufactured, which were divided into 1 set of specimens with 1 single hole and 3 sets of specimens with 4 holes. The specific dimensions are shown in Table 1, Figs. 1 and 2. Q345 bridge steel with a thickness of 12 mm was adopted by the perforated steel plate while the I-section was adopted by the steel structure. Q345 bridge steel has better impact toughness than normal Q345 steel and is widely used in steel structure bridge construction. The perforated steel plate and steel structure was welded with each other. The diameter of the hole was designed to be 60 mm. HRB400 and HPB300 were adopted as the transverse reinforcement and lateral reinforcement with a diameter of 8 mm, respectively.

The I-section beam was ribbed in order to prevent local buckling. Moreover, the lubricating oil was applied to the flange plate at the intersection of the I-beam and the concrete to eliminate the influence of the cohesive force before the specimen was poured.

Table 1. Dimensions of PBL Shear Connectors

Specimen number	Diameter of transverse reinforcement/mm	Hole diameter/mm	Number of holes on each side
SB21	ϕ20	60	1
SB12	ϕ16	60	4
SB22	ϕ20	60	4
SB32	ϕ25	60	4

Note: SB represents specimen; the first number represents diameter, 1/2/3 corresponding steel bars of 16/20/25 mm; the second number represents the type of holes, 1 to one hole, 2 to four holes.

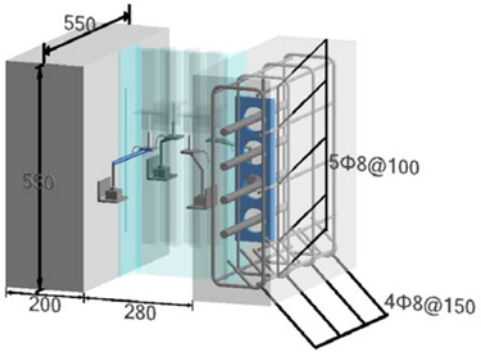

Fig. 1. Schematic Diagram of the Specimen in Push-Out Test (mm)

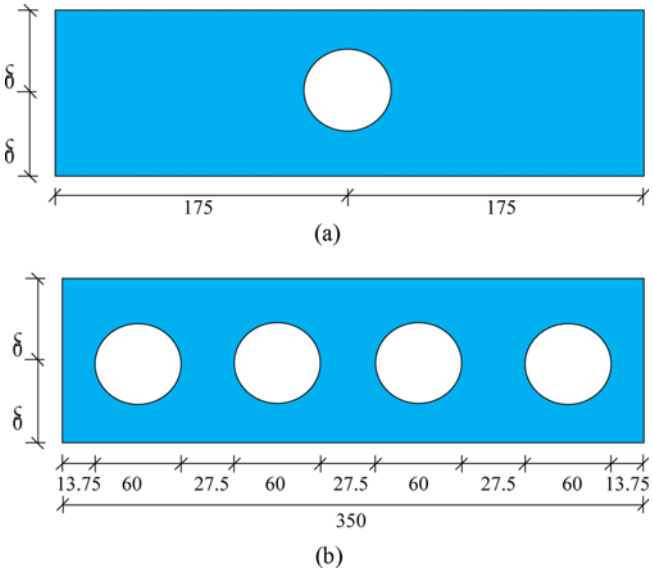

Fig. 2. Schematic Diagram of the Perforated Steel Plate (mm): (a) Specimen with 1 Single Hole, (b) Specimen with Four Holes

2.2 Loading and Measurements

The standard concrete specimen was tested for compressive strength by a high-stiffness loading instrument with the compress loading of 3,000 kN. The tensile strength is tested by an electronic

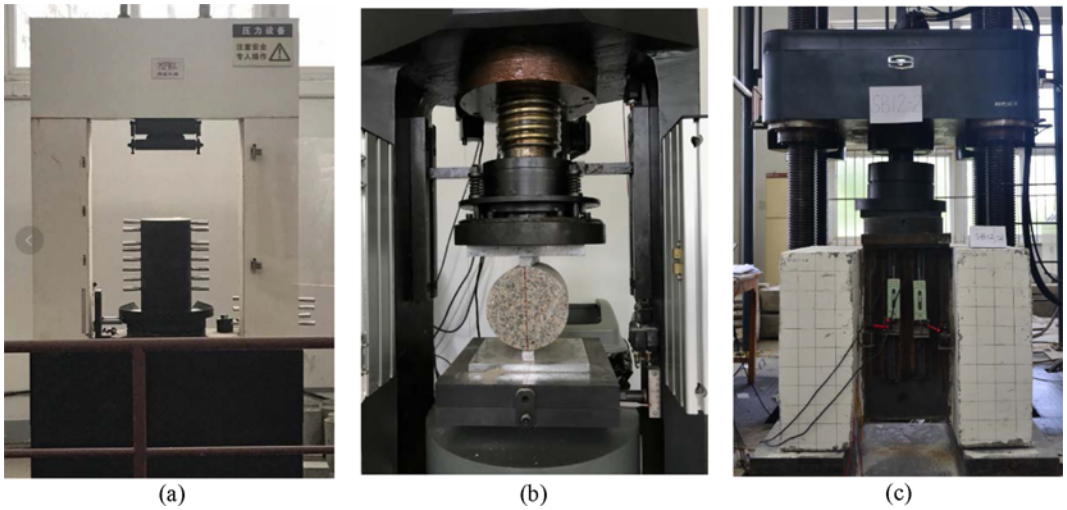

Fig. 3. Test Equipment: (a) High Stiffness Rock Press, (b) Electronic Universal Servo Testing Machine, (c) Servo Long Column Tester

Table 2. Mix Proportion of UHPC

Water-binder ratio	Water (kg/m^3)	Cement (kg/m^3)	Steel fiber ($\%/m^3$)	Silica fume (kg/m^3)	Sand (kg/m^3)	coarse aggregate (kg/m^3)	Admixtures (kg/m^3)
0.18	135	670	1.5	80	750	875	15.0

servo test machine with the tension loading of 2,000 kN. The push-out specimen was loaded by a servo long column test machine with the loading of 5,000 kN. The instruments are shown in Fig. 3. The loading of the test was divided into three stages. The first stage was preloaded to 50 kN to ensure that the surfaces of the specimen were tightly fitted to each other. After that the testing instruments were reset to zero and then loaded to 100 kN by force control at the rate of 1.2 kN/s. Then the specimen was loaded to 350 kN, cycled three times to eliminate the effect of elastic strain. Force control was used to accurately control the load increment and prevented the force from rising too fast due to displacement control. During the second stage, displacement control with 0.012 mm/s was adoptee to a displacement of 30 mm. Finally, displacement control with 1 mm/min was adopted again to failure during the third stage.

The ultimate load of the concrete specimen was directly obtained by the test machine, and then substituted into the formula to calculate the concrete compressive strength and tensile strength. The applying load and the relative slip of the steel plate and the concrete were tested during the push-out test. The applying load can be directly obtained from the testing machine, while the relative slip was obtained by the four displacement monitor metrically arranged before and after the specimen and connected to the data acquisition instrument.

2.3 Materials Properties

The mix proportion of UHPC is shown in Table 2. The coarse aggregate made of basalt with a particle size of less than 13.5 mm was provided by an asphalt mixing plant in Jurong, China. This is supported by the study which showed that the basalt can reinforce the strength of the concrete (Liu et al., 2013). The fine aggregate was medium sand with a particle size of less than 5 mm and the fineness modulus of sand was 0.19. The silica fume was nano-silica, the cement of PII grade Portland cement, the fly ash of grade I ash. The diameter of steel fiber that made of copper-plated microfilament was 0.28 mm with the length of 35 mm and the test report provided by vendor showed that the tensile strength of steel fiber can reach 2850 MPa. To improve the performance of concrete, a high-performance poly carboxylate water reducer was adopted.

Table 3. UHPC Properties

Specimen number	Compressive strength /MPa	Tensile strength /MPa	Elastic modulus /MPa
SB-1	152.3	14.2	5.1×10^4
SB-2	148.6	14.8	5.1×10^4
SB-3	155.4	14.3	5.1×10^4
Average	152.1	14.4	5.1×10^4

Fluidity measurements were required before each pouring.

In this paper, the section of UHPC is compared with the general concrete by MATLAB through binary image method, as shown in Fig. 4. Among the figures, the black solid irregular mass in Figs. 4(a) and 4(b) is coarse aggregate, and the blank is cement slurry. As shown in the figure, the UHPC coarse aggregate has a smaller particle size and a uniform distribution, and the steel fibers are also dispersed in various corners of the cement slurry. In the general concrete, the coarse aggregate has relatively larger particle size and the aggregate is not active. It only relies on the "unilateral growth effect" to form the ITZ zone, and the "boundary" effect is more obvious, which makes it easy to form the concentration gradient of the cement slurry, and make the ITZ zone less dense. UHPC can reduce the influence of the "boundary" effect effectively due to the addition of silica fume-assisted cementitious materials. Therefore, compared to general concrete, UHPC has higher compressive strength, tensile strength and better performance to inhibit crack growth and expansion.

3. Test Results

3.1 Failure Modes

In this test, specimens with a single hole and specimens with four

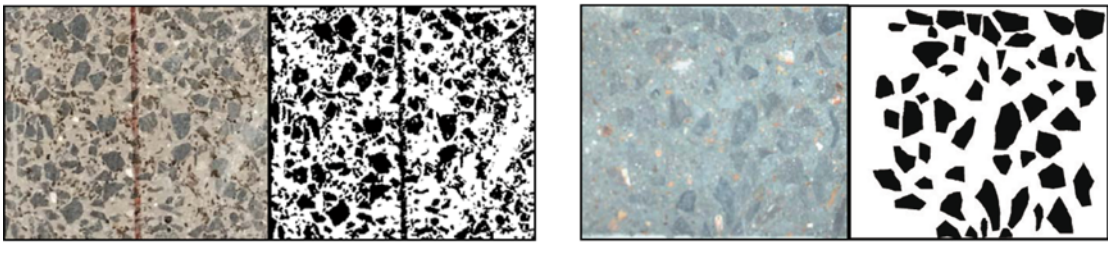

(a) (b)

Fig. 4. Comparison of UHPC and Normal Concrete Sections: (a) Sectional View of UHPC Specimen in This Paper, (b) Sectional View of Normal Concrete

holes shared similar failure modes. Before loading to 70% of the ultimate load, the specimen only showed a slight rustle sound. As the load gradually approached the ultimate load, the rustle sound gradually became louder. Meanwhile, the concrete dowel is mainly subjected to shear force, and the rustle sound indicated the sound of the concrete squeezing. When approaching the ultimate load, the rustle sound is further louder. At this time, it can be considered that the concrete dowel has failed, the transverse rebar mainly offered the shear resistance. However, the load will not increase dramatically due to the decrease of the overall stiffness. The bearing capacity of the specimen was basically stable, fluctuating within an interval called the holding phase. At this stage, due to the steel fiber inside, the UHPC depressed new internal cracks so that no cracks appeared on the surface. Meanwhile, the strain energy accumulated inside the specimen cannot be released due to the crack being suppressed. As the test continued, the strain energy accumulated on the steel bars that depressed the relative slip of the test piece. As the transverse rebar reached the ultimate strength, a loud noise occurred with the first transverse rebars nipped. Due to the chain effect and the stress concentration, the residual transverse rebars were cut through one by one within a short time, and the strain energy is released at the crack end resulting in a new crack. This is the mechanism that when UHPC is tested, the crack generally appeared after the transverse rebars were cut through. As more transverse rebars were cut through, the cracks spread faster. As is shown in Fig. 5, cracks mainly appeared on the top and bottom of the specimen, and the corresponding failure mode showed a longitudinal splitting failure trend.

Because the development trend of cracks was similar, and most of the cracks appeared in the same part, which showed that the influence of other minor factors can be excluded, and the most critical failure modes can be presented. Therefore, UHPC can be used as an ideal material to study the most basic force transfer mechanism of PBL shear connectors. It can also be seen from Fig. 5(c) that although the specimens showed obvious relative slip, the cracks were of small amount and the occurrence is the same, which showed that UHPC could suppress the development of cracks efficiently. When used in engineering practice, these small cracks can be reinforced in advance to extend the service time of the construction.

3.2 Load-Slip Curve

The load-slip curves of the specimens are shown in Fig. 6, and the relative slips were obtained by the average of the four displacement meters.

The specimen with a single hole is the basis for studying its mechanical properties, and its load-slip curve also provides a theoretical model basis for the subsequent finite element analysis. As shown in Fig. 6(a), the load of the specimen with a single hole increased linearly to the peak load at the initial stage. After that the load was reduced to 50% of the ultimate capacity and kept. Therefore, the shear stiffness provided by the shear connector was mainly effective within the initial stage. The load corresponding to the slip of 0.5 mm was the ultimate load, which can be used as a reference for the conservative design of the shear connector. However, it is infeasible to carry shear force only by a single shear connector in engineering practice. Therefore, it requires the study based on the shearing mechanism and the force transmission mode of the specimen with a single hole, and then extended to reasonable design based on the specimen with several holes.

Except for the single-hole SB21 specimen, the curves of the other three sets of specimens with four holes were relatively similar, which could be divided into four stages: I-the linear elastic stage, II-the initial plastic stage, III-the yield strengthening stage and IV-the post peak stage. The load-slip curve of the maximum ultimate bearing capacity of each group of specimens is taken as an example, and the division of four stages is shown in Fig. 6. The initial plastic stage corresponds to approximately between 75% and 85% of the peak load and each specimen has a different value. When the initial slip was small, the load increases linearly and rapidly, and the shear stiffness maintained a high level. Once the initial plastic stage is reached, the load growth rate slowed down until the yield strengthening stage was reached when the load growth further significantly slowed down. When the ultimate load was reached, the curve began to decrease slowly until the specimen is destroyed completely. Considering

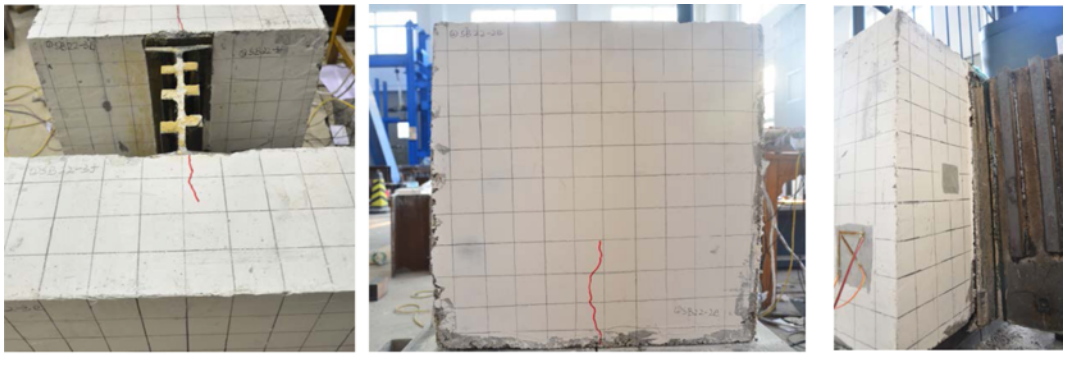

Fig. 5. Test Situation of Specimens: (a) Top Cracks, (b) Side Cracks, (c) Slip Interface

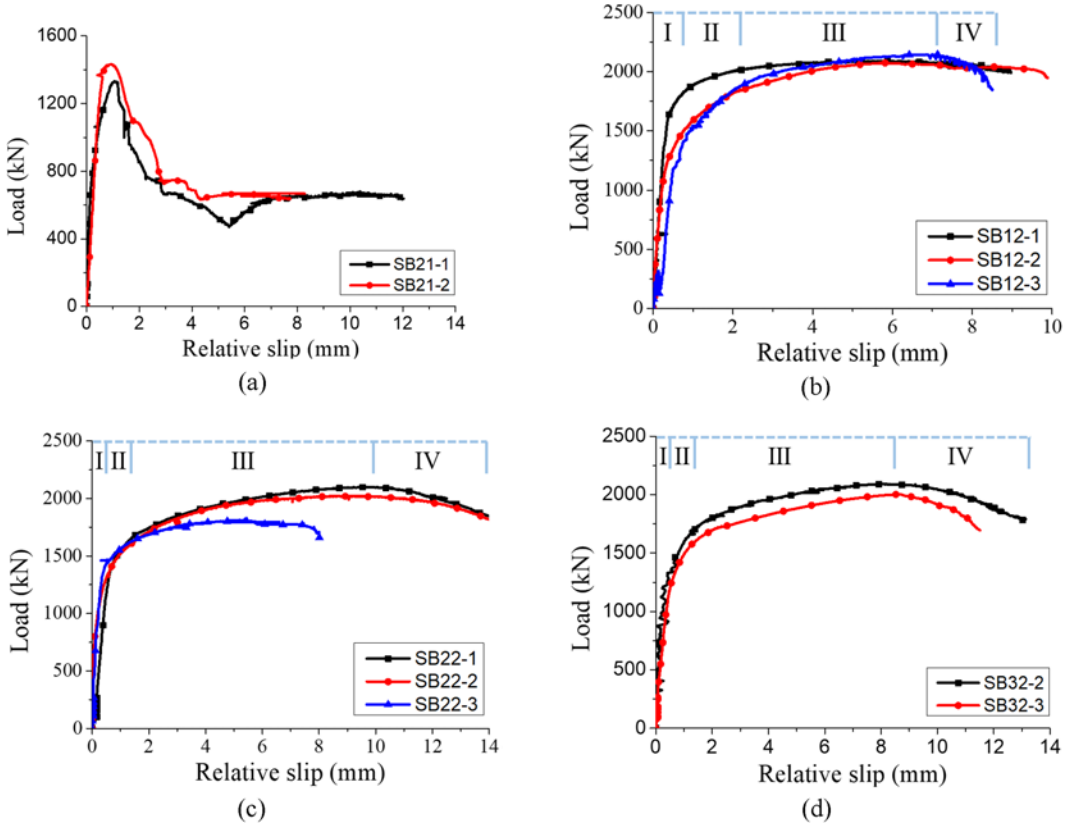

Fig. 6. Load-Slip Curves: (a) SB21, (b) SB12, (c) SB22, (d) SB32

that the specimen is no longer applicable in engineering practice when it reaches the post peak stage, the curve is selected from outset to a small section after reaching the post peak stage. It can be seen from the figure that the ultimate bearing capacity of the specimen with four holes was approximately 2,000 kN, which was only 42.8% higher than the specimen with a single hole. Because perfobond rib shear connector with UHPC acquired a balance between the concrete dowel and the transverse rebar, the increase of the diameter of the transverse rebar lead to a reduction in the area of the concrete dowel, so a larger diameter of the transverse rebar did not always perform more effectively. The force transmission mechanism is more complicated for UHPC, therefore the relative increase of bearing capacity of the specimen with four holes was not as remarkable as expected. Besides, the spacing between adjacent holes providing shear was smaller, and the probability of mutual influence of each factor will be dramatically increased, making the shear connector could not be fully utilized, and failure occurred in advance.

Due to the failure of the test machine, the SB21-3 specimen and the SB32-1 specimen are not described here.

4. Calculation Formula of Ultimate Capacity

The study of the ultimate capacity formula has always been an important part of the PBL shear connectors. For example, Oguejiofor and Hosain (1997), Medberry and Shahrooz (2002), Vianna et al. (2013), Hosaka et al. (2002), Zhu et al. (2019) and other scholars have proposed corresponding bearing capacity calculation formula. These formulas have one thing in common, that is, the bearing capacity of perfobond rib connector is provided by concrete dowel, transverse rebar and stirrups. Therefore, the calculation formula is generally composite of three parts, as shown in the Eq. (1).

$$Q_u = \alpha A_{tr} f_y + \beta A_c f_c + \gamma A'_{tr} f'_y \quad (1)$$

where A_{tr} is the area of the transverse reinforcement, f_y is the yield strength of the transverse reinforcement, A_{tr}' is the area of the lateral reinforcement, f_y' is the yield strength of the lateral reinforcement, A_c is the area of the concrete dowel, and f_c is the compressive strength of the cylinder concrete, Among them, α, β and γ are the influence coefficients obtained by regression analysis.

The formulas above are all for general concrete. The selected parameters of concrete can be considered as the critical state of concrete dowel crushing. At this time, certain cracks have been generated in the concrete. For PBL shear connectors with UHPC, the concrete dowel as well as the steel fibers both contributes to shear resistance. For general concrete, the concrete dowel is squeezed to produce cracks and then rapidly expands into brittle fractures through the cracks. However, there are steel fibers with uniform and irregular distribution in UHPC, which dramatically influence the capacity of inhibition of cracks. When the concrete

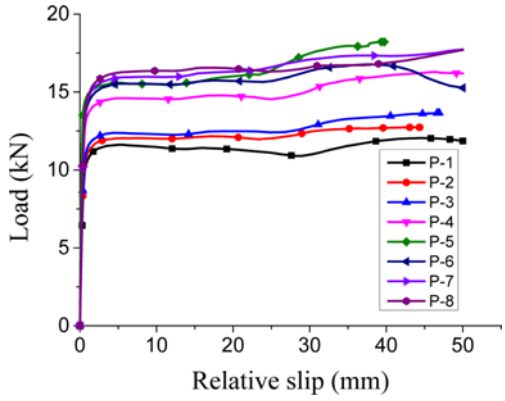

Fig. 7. Load-Slip Curve of Each Specimen

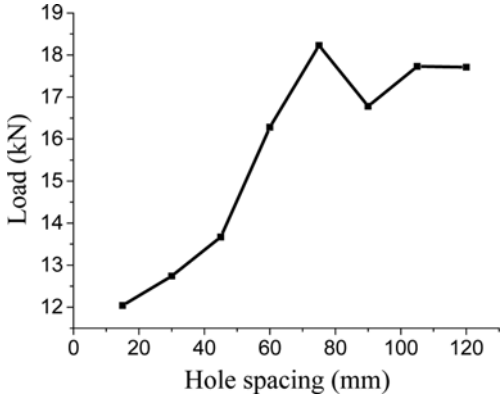

Fig. 8. Comparison of Ultimate Bearing Capacity of Each Specimen

dowel can no longer carry the load, the steel fiber is tightly restrained by the bonding force with the concrete, which delays the further cracking of the concrete dowel.

The role of the stirrups is to limit the local cracking of the concrete and maintain the integrity of the concrete. However, it can be seen from the above test phenomenon that the crack appeared on the concrete surface after the limit load reached. In the early stage, the steel fiber is more resistant to cracking, so the contribution of the stirrup to the shear is negligible relative to the steel fiber.

Based on the improvement of the existing formula, this paper carries out fitting analysis on the measured peak load in this paper.

Based on modification of the existing formula and in view of the contribution of steel fiber shear resistance, the following formula is carried out by fitting analysis on the measured data in this paper.

$$Q_u = \xi\left(0.52A_c f_c + 0.12A_{tr} f_y + 0.13A_{fr} f_{fr}\right) \tag{2}$$

where ξ is the hole characteristic coefficient, which shows that the bearing capacity of specimen with several holes is not accumulation of bearing capacity, and a certain reduction appears. $\xi = -0.55n + 3.2$, where n is the number of single-sided holes; A_{tr}, A_c, f_c, f_y have the same meaning as before, but they are all correspond to single hole; f_{fr} is the resistance of steel fiber tensile strength; A_{fr} is the converted cross-sectional area of steel fiber in single hole, which can be calculated by the following method.

Oguejiofor and Hosain (1997) shows that the "interlocking effect" of the PBL shear connector can be eliminated when the hole spacing of the two holes is greater than 2.25 times of the diameter of the holes. To verify this, the influence of the hole is analyzed by ABAQUS. The half-side PBL shear connector is adopted to construct the specimen. The hole spacing is increased by a step of 15 mm from 15 mm to 120 mm, totally 8 specimens. The specimens are named P1 – P8. The hole spacing here refers to the distance between the outermost edges of the two holes. The purpose of modeling is to obtain the influence of hole spacing on ultimate bearing capacity. Therefore, in order to simplify the calculation, the elastic model is used and the young's modulus is measured by experiments. At the same time, the effect of steel fibers on concrete is not considered conservatively. The effect of through reinforcement is also ignored, because the insertion of through reinforcement will increase the overall bearing capacity and stiffness, and the region of influence on the surrounding concrete will be smaller.

The ultimate bearing capacity of each specimen is shown in Fig. 8. It can be seen clearly that the bearing capacity reaches a maximum value when the hole spacing is 75 mm, and the bearing capacity increases obviously with the increase of spacing when the distance is less than 75 mm. But the improvement is relatively less unconspicuous after the 75 mm space.

The finite element calculation results are consistent with the results of the Oguejiofor's study, which indicate that the shear connector affects the surrounding concrete range of 1.125 times of the diameter of the hole. In this paper, it is a sphere with a diameter of 67.5 mm as the origin of the hole center, so the first calculation is the volume V_c, which is the volume of the concrete minus the volume of the perforated steel plate therein. The calculation formula is then shown as Eq. (3).

$$A_{fr} = \frac{\rho V_c}{L} \tag{3}$$

where ρ is the volume fraction of the steel fiber and L is the diameter of the sphere, which is equivalent to simplifying all the steel fibers in this volume range to be gathered in a straight line along the direction of the through-bar, thereby suppressing the shear failure of the concrete dowel. After that, divided by the diameter L of the sphere, the converted cross-sectional area of the steel fiber is obtained. Fig. 9 shows the schematic diagram of the formula.

In order to demonstrate the feasibility of the formula, the calculation models of ultimate bearing capacity proposed by some scholars are selected in this paper (Table 4).

As shown in Table 4, it is found that the calculation results calculated in this paper agree well with the experimental values. The equation proposed by Oguejiofor overstates the contribution of concrete, as the strength of concrete increases, the ultimate bearing capacity increases linearly. This is also due to the little attention on high strength concrete in the early period. The rest of the

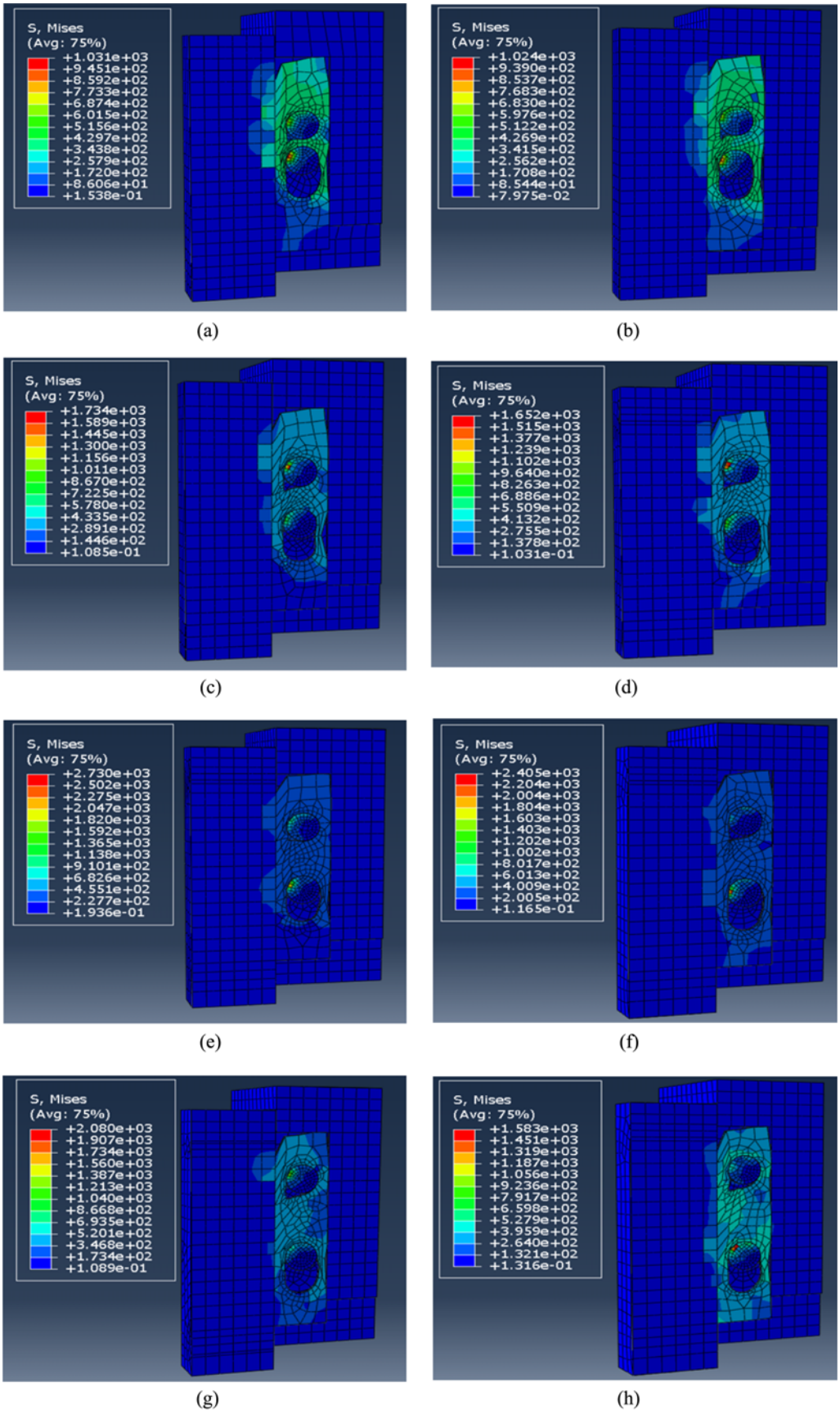

Fig. 9. Hole Influence Finite Element Calculation Cloud Figure (MPa): (a) P1, (b) P2, (c) P3, (d) P4, (e) P5, (f) P6, (g) P7, (h) P8

Table 4. Perfobond Connector Calculation Formulas Proposed by Different Authors

Authors	Models	Equation
Medberry	$Q_u = 0.747bh\sqrt{f_c} + 0.413b_f L_c + 0.9A_{tr}f_y + 1.66n\pi\left(\frac{D}{2}\right)^2\sqrt{f_c}$	(4)
Vianna	$Q_u = 31.8 + 1.9\times10^{-3}\times htf_c + 0.53\times10^{-3}\times A_{tr}f_y - 0.6\times10^{-6}\times A_c\sqrt{f_c}$	(5)
Oguejiofor	$Q_u = 4.5htf_c + 0.91A_{tr}f_y + 3.31nD^2\sqrt{f_c}$	(6)
Hosaka	$Q_u = 1.45\left[\left(D^2 - d^2\right)f_c + d^2 f_y\right] - 26.1$	(7)
Zhu	$Q_u = 2\left(1 + r_m \times s\right)l_m \times t \times f_u$	(8)
	$r_m = \begin{cases} 0 & e_s < 0.7e_b \\ 1 & e_s > 0.7e_b \end{cases}$	(9)

Table 5. The Comparison of Calculation Formulas between Some Scholars and This Paper

Specimen number	Test value /kN	Medberry/Vianna /kN	Oguejiofor /kN	Hosaka /kN	Zhu /kN	Proposed formula /kN
SB12-1	260.5	138.2	151.9	442.9	174.2	198	277.6
SB12-2	259.3						
SB12-3	268.0						
SB21-1	665.0	223.1	503.6	1203.9	755.7	648	731.4
SB21-2	716.0						
SB22-1	262.3	178.9	175.8	484.0	188.9	198	276.0
SB22-2	252.6						
SB22-3	226.3						
SB32-2	261.1	242.5	213.3	548.4	211.9	198	273.6
SB32-3	250.4						

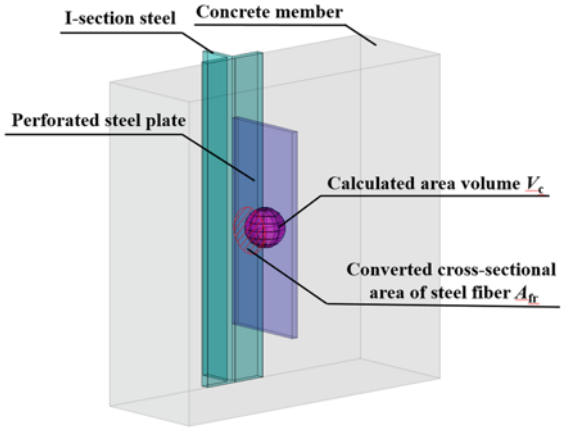

Fig. 10. A Schematic Diagram of Eq. (3)

formulas underestimate the results, mainly for the following reasons:

1. All of them are based on normal concrete and the contribution of steel fibers are ignored. In fact, the tensile strength of concrete improved by steel fiber have a significantly influence on cracking performance.
2. Medberry and Vianna consider the contribution of steel plate, concrete dowel and transverse steel bars. However, the bond performance is not shown in these equations. If the influence of steel plate is mentioned, the bond performance should not be ignored because of the large contact surface between concrete and steel plate. Moreover, Eq. (5) underestimate the contribution of concrete. As we can see in the last item, the order of magnitude is too small.
3. Hoska take consider of the contribution of concrete dowel and transverse steel bars. This formula takes too few factors into account and it is easy to underestimate the ultimate bearing capacity. Zhu simplifies the traditional equation model and only consider the influence of steel plate. He thinks that the fracture of steel plate causes the failure of PBL shear connector. This formula works well for specimens with holes close to the edge of the steel plate, but there is a deviation for calculation results under other types of PBL specimens.

5. Calculation Formula for Shear Stiffness Based on Timoshenko Beam

The ultimate bearing capacity calculation formula can only calculate the bearing capacity under the limit state. In order to evaluate the performance during the service period, the member during the service period can be approximated considered as the elastic stress state. Therefore, the initial shear stiffness can calculate the corresponding bearing capacity of any displacement.

Yang and Chen (2018) derived the initial shear stiffness formula from the micro-segment angle using the Euler-Bernoulli beam element. Euler-Bernoulli beams are usually used for beams of large depth-span ratio, but the concrete dowels of this paper are 400 mm in length and 60 mm in diameter, which is no longer a “shallow beam”. At this time, the shear force of the beam will produce shear deformation, which causes additional deflection so that the plane section assumption is not fully applicable. The Timoshenko beam element can effectively solve this problem, So the Timoshenko beam element is used to calculate the full curve in order to obtain a more accurate solution.

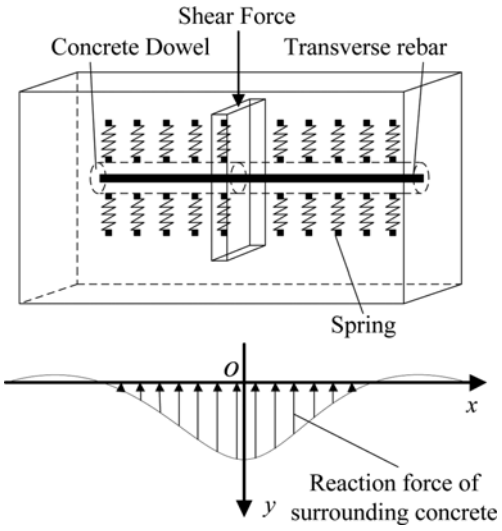

Fig. 11. Theoretical Model and Deformation Curve of Elastic Foundation Beam

The concrete dowel and the transverse reinforcement are considered as separators, and the separator is subjected to vertical shearing force at the hole. The supporting reaction force is provided by the surrounding concrete. Through the analysis of the experimental phenomena, it can be seen that the failure of PBL shear connector is mainly the shearing of the transverse rebar, and the slight deformation only occurs in the elastic stage. The capacity of this deformation to diffuse to both ends is limited, so it can be equivalent to an infinite length elastic foundation beam. The schematic diagram of the model is shown in Fig. 11.

The surrounding outer concrete is a continuous elastic material, therefore the support stiffness per unit length can be defined as $k = CE_c$, where C is the undetermined constant 1. The assumptions are made before calculating the shear stiffness as follows:

1. The stiffness of the equivalent spring is proportional to the modulus of elasticity of the concrete.
2. The influence of the adhesion between the perforated steel plate and the concrete is neglected.
3. The reaction force of the concrete is proportional to the deformation of the insulation.
4. The transverse rebar and concrete dowel only carry the concentrated shear force transmitted through the upper end.
5. The section perpendicular to the neutral axis remains flat after deformation but is not perpendicular to the neutral axis.

The element micro-section of Timoshenko beam is shown in Fig. 12. In addition to the rotation angle θ caused by the bending deflection, it considers the section rotation angle caused by the shear deformation of the beam. The deflection y corresponds to the external load q, and the corner angle ψ corresponds to the distribution moment m, of which direction is positive clockwise.

$$\begin{cases} M = -EI\dfrac{\mathrm{d}\psi}{\mathrm{d}x} \\ Q = \mu GA\gamma \end{cases} \tag{10}$$

where EI is the bending stiffness, μGA is the shear stiffness and μ is the shear correction coefficient of beam section.

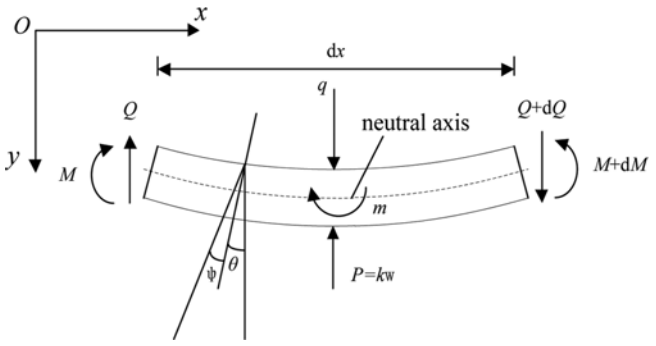

Fig. 12. Micro-Segment Model of Elastic Foundation Beam Using Timoshenko Beam Theory

Two basic equilibrium equations can be derived as follows:

$$\begin{cases} \dfrac{\mathrm{d}Q}{\mathrm{d}x} + q = P \\ -\dfrac{\mathrm{d}M}{\mathrm{d}x} + Q + m = 0 \end{cases} \tag{11}$$

Substituting the various parameters of this paper, Eq. (12) is available.

$$\begin{cases} -\dfrac{d}{dx}\left[K_s\left(\dfrac{d\omega}{dx} - \psi\right)\right] + k\omega = q \\ \dfrac{d}{dx}\left(K\dfrac{d\psi}{dx}\right) + K_s\left(\dfrac{d\omega}{dx} - \psi\right) = -m \end{cases} \tag{12}$$

where K_s is the shear stiffness of the comparison beam, K is the bending stiffness of the comparison beam, and ω is the deflection of the comparison beam.

After calculation, the analytical solution of the comparative beam internal force can be obtained as follows:

$$\begin{cases} \omega = \dfrac{P\alpha}{4k}\cdot F_1(x) \\ \psi = -\dfrac{P}{4K\alpha\beta}\cdot F_2(x) \\ Q = -\dfrac{P}{2}\cdot F_3(x) \\ M = \dfrac{P}{4\alpha}\cdot F_4(x) \end{cases} \tag{13}$$

Where,

$$\begin{cases} F_1(x) = e^{-\alpha x}\left[\dfrac{\left(3\alpha^2 - \beta^2\right)}{\alpha^2}\cos\beta x + \dfrac{\left(3\beta^2 - \alpha^2\right)}{\alpha\beta}\sin\beta x\right] \\ F_2(x) = e^{-\alpha x}\sin\beta x \\ F_3(x) = e^{-\alpha x}\left[\cos\beta x + \dfrac{\left(\beta^2 - \alpha^2\right)}{2\alpha\beta}\sin\beta x\right] \\ F_4(x) = e^{-\alpha x}\left[\cos\beta x - \dfrac{\alpha}{\beta}\sin\beta x\right] \end{cases} \tag{14}$$

Where,

$$\alpha = \sqrt{\sqrt{\frac{k}{4K}} + \frac{k}{4K_S}} \qquad \beta = \sqrt{\sqrt{\frac{k}{4K}} - \frac{k}{4K_S}} \tag{15}$$

According to the Timoshenko beam theory, the deflection of the shear beam is composed of bending and shearing. Therefore, in order to obtain the shear stiffness, the formula of the deflection curve can be obtained. When the shear force V acts directly above the perforated steel plate, i.e. $x = 0$, the relative slip between the concrete and the perforated steel plate is as follows:

$$\omega = \frac{P\alpha}{4k} e^{-\alpha x} \left[\frac{\left(3\alpha^2 - \beta^2\right)}{\alpha^2} \cos \beta x + \frac{\left(3\beta^2 - \alpha^2\right)}{\alpha\beta} \sin \beta x \right] \tag{16}$$

It can be seen from Eq. (16) that the relationship between the deflection of the beam and the shear force is related to K_s, therefore the shear stiffness can be calculated by:

$$K_s = \frac{4k}{\alpha} \tag{17}$$

The shear stiffness in the hole is mainly provided by concrete dowel and transverse reinforcement. The bending stiffness is calculated by the inertia moment calculation formula analogy of the elastic foundation beam.

$$K = E_c \frac{\pi}{64}\left(d^4 - d_s^4\right) + E_s \frac{\pi}{64} d_s^4 \tag{18}$$

Further rewriteable as:

$$K = \pi E_c d^4 \left[1 + \left(n_E - 1\right) n_d^4\right] / 64 \tag{19}$$

where n_E is the ratio of the elastic modulus E_s of the transverse reinforcement to the elastic modulus E_c of the concrete, and n_d is the ratio of the diameter of the transverse reinforcement and the diameter of the hole of the perforated steel plate.

Substituting Eq. (19) and α into Eq. (17), the shear stiffness of the perforated steel plate connector can be calculated by:

$$K_s = \sqrt{\frac{\sqrt{K^2 + 4096kK} - K}{8}} \tag{20}$$

Based on the assumption that the concrete is compared to the elastic foundation, the stiffness is mainly related to the elastic modulus of the concrete, while the stiffness of the composite beam is mainly provided by concrete and steel. When UHPC is applied, the elastic modulus of the two is in the same order of magnitude, but the number 4096 of the middle root number in Eq. (20) is already three orders of magnitude larger than the previous one, so Eq. (20) can be approximately rewritten as:

$$K_s = \sqrt{\frac{\sqrt{4096kK} - K}{8}} \tag{21}$$

Equation (19) be converted to Eq. (20), where $T = 1 + \left(n_E - 1\right) n_d^4$.

$$K_s = \sqrt{\frac{512\sqrt{\pi C} E_c d^2 \sqrt{T} - \pi E_c d^4 T}{512}} \tag{22}$$

The constant term in Eq. (22) can be replaced by β_1, and

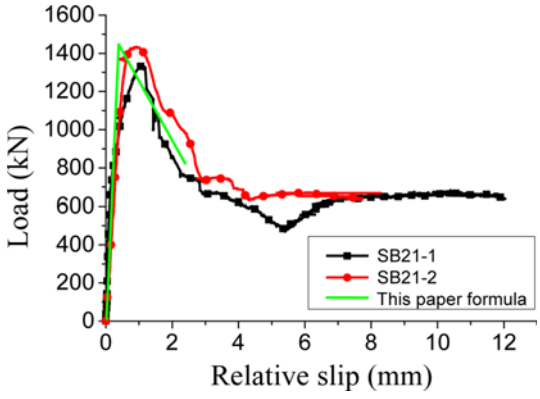

Fig. 13. Comparison between Tested Stiffness and Calculations

$\beta_1 = 13868$ is calculated. Therefore, the final expression of the shear stiffness K_s based on Timoshenko beam can be calculated by:

$$K_s = \sqrt{\frac{13868 E_c d^2 \sqrt{T} - \pi E_c d^4 T}{512}} \tag{23}$$

In this calculation, only the elastic stage and the curve reaches about 2.5 mm after the peak load are considered, as can be seen in Fig. 5(a).

Analogous to the initial shear stiffness of open-walled steel joints, the concept of final shear stiffness can be defined at this point. The shear stiffness of the last-time perforated steel plate is mainly provided by the concrete dowel. The combined bending stiffness of the elastic foundation beam can be calculated by:

$$K_T = \pi E_c d^4 / 64 \tag{24}$$

Substituting Eq. (24), $k = CE_c$, and α into Eq. (17), and using C instead of the constant term in the shear stiffness equation, the shear stiffness of the perforated steel plate joint is as follows:

$$K_{ST} = C_1 E_c d\left(d + \sqrt{d^2 + 1}\right) + C_2 \tag{25}$$

$C_1 = -7.3 \times 10^{-3}$, $C_2 = 1270$ are obtained by linear fitting of the data measured in the Nanjing Forestry University civil engineering laboratory, so the final shear stiffness is:

$$K_{ST} = -7.3 \times 10^{-3} E_c d\left(d + \sqrt{d^2 + 1}\right) + 1270 \tag{26}$$

Therefore, the load-slip full curve model expression of the perfobond rib connector with UHPC is Eq. (27).

$$P = \begin{cases} sK_s & 0 \le s \le 0.5 \text{ mm} \\ sK_{sT} & 0.5 \text{ mm} \le s \le 2.5 \text{ mm} \end{cases} \tag{27}$$

The calculated results are in good agreement with the experimental data (Fig. 13). Considering that the elastic limit state is generally considered in practical applications, this formula can determine the ultimate bearing capacity from the stiffness angle and has practicality.

6. Conclusions

This study presents a summary of experimental and theoretic results of PBL shear connectors consisting of two types of specimens with UHPC. Based on experimental load-slip curves, numerical analysis, and an analytical model based on the Timoshenko beam. The following conclusions can be drawn:

1. The pull-out test of PBL shear connector with UHPC can be divided into four stages: elastic, initial plastic, yield strengthening, post peak. PBL shear connector with UHPC has higher redundancy because of a long period of yield strengthening.
2. The PBL shear connecter using UHPC is mainly disable for concrete crushing and the fracture of transverse bars. Few surface cracks are occurred on the surface and are all concentrated on the plate axis. In the actual project, the crack development trend can be directly judged and the designated location can be strengthened in advance.
3. The steel fiber in UHPC takes on more shear resistance, this paper proposes the calculation formula of ultimate capacity based on the concept of steel fiber conversion cross-sectional area.
4. According to the elastic foundation beam method, the initial shear stiffness of the single-hole PBL shear bond is calculated by Timoshenko beam element, and the load-slip relationship calculation formula is obtained.

Acknowledgements

The authors wish to express their sincere to the Innovation and Entrepreneurship Training Program for Students (201710298024Z) for their financial support. Furthermore, they also want to express great thanks to the researchers of Civil Engineering Laboratory at Nanjing Forestry University for their support during this research program.

ORCID

Maojun Duan https://orcid.org/0000-0002-1459-4538
Shiyu Zhang https://orcid.org/0000-0002-4537-7536
Xu Wang https://orcid.org/0000-0002-3527-4285
Fenghui Dong https://orcid.org/0000-0002-3315-6699

References

Aaleti S, Petersen B, Sritharan S (2013) Design guide for precast UHPC waffle deck panel system, including connections. No. FHWA-HIF-13-032. Federal Highway Administration, Washington, DC, USA

Al-Shuwaili MA (2018) Analytical investigations to the specimen size effect on the shear resistance of the perfobond shear connector in the push-out test. *Procedia Structural Integrity* 17:1924-1931, DOI: 10.1016/j.prostr.2018.12.269

Chen BC, Mou TM, Chen YY, Huang YZ (2013) State-of-the-art of research and engineering application of steel-concrete composite bridges in China. *Journal of Building Structures* 17(1):1-10, DOI: 10.14006/j.jzjgxb.2013.s1.006 (in Chinese)

Chung CH, Lee J, Kim JS (2016) Shear strength of t-type perfobond rib shear connectors. *KSCE Journal of Civil Engineering* 20(5):1824-1834, DOI: 10.1007/s12205-015-0095-8

Di J, Zou Y, Zhou XH, Qin FJ, Peng X (2018) Push-out test of large perfobond connectors in steel–concrete joints of hybrid bridges. *Journal of Constructional Steel Research* 150:415-429, DOI: 10.1016/j.jcsr.2018.09.002

EUROCODE 4 (2004) Design of composite steel and concrete structures. British Standards Institution, London, UK

He SH, Fang Z, Mosallam AS (2017) Push-out tests for perfobond strip connectors with UHPC grout in the joints of steel-concrete hybrid bridge girders. *Engineering Structures* 135:177-190, DOI: 10.1016/j.engstruct.2017.01.008

He SH, Mosallam AS, Fang Z, Zou C, Feng WX, Su J (2018) Experimental study on CFSC encased shear connectors in steel-concrete composite joints with UHPC grout. *Construction and Building Materials* 173:638-649, DOI: 10.1016/j.conbuildmat.2018.04.086

Hosaka T, Mitsuki K, Hiragi H (2002) Study on shear strength and design method of perfobond strip. *JSCE Committee of Structural Engineering* 48:1265-1272

Huh SB, Byun YJ (2005) Sun-Yu pedestrian arch bridge, Seoul, Korea. *Structural Engineering International* 15(1):32-32, DOI: 10.2749/101686605777963378

Kim SH, Han O, Kim KS, Park JS (2018) Experimental behavior of double-row y-type perfobond rib shear connectors. *Journal of Constructional Steel Research* 150:221-229, DOI: 10.1016/j.jcsr.2018.08.012

Leonhardt F, Andra W, Andra W, Andrae EFW, Andra HP, Harre W (1987) Neues, vorteilhaftes verbundmittel für stahlverbund-tragwerke mit hoher dauerfestigkeit. *Beton-und Stahlbbetonbau* 82(12):325-331, DOI: 10.1002/best.198700500 (in German)

Li WG, Shao XD, Fang H, Zhang Z (2015) Experimental study on flexural behavior of steel-UHPC composite slabs. *China Civil Engineering Journal* 48(11):93-102, DOI: 10.15951/j.tmgcxb.2015.11.013 (in Chinese)

Li ZX, Zhao CH, Deng KL, Wang WA (2018) Load sharing and slip distribution in multiple holes of a perfobond rib shear connector. *Journal of Structural Engineering* 144(9):04018147, DOI: 10.1061/(ASCE)ST.1943-541X.0002152

Liu LB, Zhang YS, Zhang WH, Liu ZY, Zhang LH (2013) Investigating the influence of basalt as mineral admixture on hydration and microstructure formation mechanism of cement. *Construction and Building Materials* 48:434-440, DOI: 10.1016/j.conbuildmat.2013.07.021

Medberry SB, Shahrooz BM (2002) Perfobond shear connector for composite construction. *Engineering Journal* 39(1):2-12

Nie JG, Tao MX, Wu LL, Nie X, Li FX, Lei FL (2012) Advance of research on steel-concrete composite bridges. *China Civil Engineering Journal* 45(6):110-122, DOI: 10.15951/j.tmgcxb.2012.06.003 (in Chinese)

Nishiumi K (1999) Shear strength of perfobond rib shear connector under the confinement. *Journal of the Japan Society of Civil Engineers* 633:193-203, DOI: 10.2208/jscej.1999.633_193

Oguejiofor EC, Hosain MU (1997) Numerical analysis of push-out specimens with perfobond rib connectors. *Computers & Structures* 62(4):617-624, DOI: 10.1016/S0045-7949(96)00270-2

Shao SD, Qu WT, Cao JH (2018) Static and fatigue properties of the steel-UHPC lightweight composite bridge deck with large U ribs. *Journal of Constructional Steel Research* 148:491-507, DOI: 10.1016/j.jcsr.2018.05.011

Shariati A (2012) Various types of shear connectors in composite structures: A review. *International Journal of the Physical Sciences* 7(22):2876-2890, DOI: 10.5897/IJPSX11.004

Su QT, Wang W, Luan HW, Yang GT (2014) Experimental research on bearing mechanism of perfobond rib shear connectors. *Journal of Constructional Steel Research* 95(3):22-31, DOI: 10.1016/j.jcsr.2013.11.020

Tanaka Y, Ohtake A, Mushi H, Watanabe N (2010) Recent innovative application of UFC bridges in Japan. Proceedings of FraMCoS-7, 7th international conference on fracture mechanics of concrete and concrete structures, May 24-27, Jeju Island, Korea, 1655-1662

Tian H, Zhou Z, Wei Y, Wang Y, Lua J (2019) Experimental investigation on axial compressive behavior of ultra-high performance concrete (UHPC) filled glass FRP tubes. *Construction and Building Materials* 225:678-691, DOI: 10.1016/j.conbuildmat.2019.07.204

Vianna J, De Andrade SAL, Vellasco PC, Costa-Neves L (2013) Experimental study of perfobond shear connectors in composite construction. *Journal of Constructional Steel Research* 81:62-75, DOI: 10.1016/j.jcsr.2012.11.002

Wang XW, Zhu B, Cui SA, Lui EM (2017) Experimental research on PBL connectors considering the effects of concrete stress state and other connection parameters. *Journal of Bridge Engineering* 23(1): 04017125, DOI: 10.1061/(ASCE)BE.1943-5592.0001158

Wei Y, Cheng X, Wu G, Duan M, Wang Libin (2019) Experimental investigations of concrete-filled steel tubular columns confined with high-strength steel wire. *Advances in Structural Engineering* 22(13): 2771-2784. DOI: 10.1177/1369433219850645

Xu X, Huang Q, Ren Y, Zhao DY, Zhang DY, Sun HB (2019) Condition evaluation of suspension bridges for maintenance, repair and rehabilitation: A comprehensive framework. *Structure & Infrastructure Engineering Maintenance Management Life-Cycle Design & Performance*, 1-13, DOI: 10.1080/15732479.2018.1562479

Yang Y, Chen Y (2018) Experimental study on mechanical behavior of PBL shear connectors. *Journal of Bridge Engineering* 23(9):04018062, DOI: 10.1061/(ASCE)BE.1943-5592.0001274

Zeng JJ, Gao WY, Duan ZJ, Bai YL, Guo YC, Ouyang LJ (2020) Axial compressive behavior of polyethylene terephthalate/carbon FRP-confined seawater sea-sand concrete in circular columns. *Construction and Building Materials* 234:117383, DOI: 10.1016/j.conbuildmat.2019.117383

Zhang QH, Jia DL, Li B, Cheng ZY, Lin X, Bu YZ (2017a) Analytical study on internal force transfer of perfobond rib shear connector group using a nonlinear spring model. *Journal of Bridge Engineering* 22(10):04017081, DOI: 10.1061/(ASCE)BE.1943-5592.0001123

Zhang QH, Jia DL, Li B, Cheng ZY, Lin X, Bu YZ (2018) Internal force transfer effect-based fatigue damage evaluation for pbl shear connector groups. *Journal of Constructional Steel Research* 148:469-478, DOI: 10.1016/j.jcsr.2018.06.016

Zhang QH, Pei SL, Cheng ZY, Yi B (2017b) Theoretical and experimental studies of the internal force transfer mechanism of perfobond rib shear connector group. *Journal of Bridge Engineering* 22(2):04016112, DOI: 10.1061/(ASCE)BE.1943-5592.0000997

Zhao C, Li Z, Deng K, Wang W (2018) Experimental investigation on the bearing mechanism of perfobond rib shear connectors. *Engineering Structures* 159:172-184, DOI: 10.1016/j.engstruct.2017.12.047

Zhu YY, Nie X, Fan JS, Cui B, Huang LJ (2019) Experimental and analytical investigation on pull-out performance of multihole thin-rib perfobond connectors. *Journal of Bridge Engineering* 24(5):04019037. DOI: 10.1061/(ASCE)BE.1943-5592.0001400